Progress In Electromagnetics Research, Vol. 148, 223–231, 2014

Investigation of Wireless Power Transfer Using Planarized, Capacitor-Loaded Coupled Loops

Chenchen Jimmy Li* **and Hao Ling**

Abstract—A capacitor-loaded coupled loop structure is investigated for wireless power transfer at 6.78 MHz for a target transmission distance of 1 m. It is shown that the optimal configuration for this structure occurs when the coupled loops are coplanar. Therefore, by converting thick wires into wide strips, a planarized configuration can be achieved. Simulation results are verified in measurement, which shows a 60% overall power transfer efficiency at 1 m. The contribution of different loss mechanisms is examined. Next, power transfer efficiency in the presence of dielectric materials is investigated in simulation and measurement. Additionally, tuning capabilities that arise from the implementation of variable capacitors are shown. Finally, design space exploration is performed to examine design tradeoffs.

1. INTRODUCTION

The demonstration of non-radiative wireless power transfer (WPT) using strongly coupled magnetic resonance reported in [1, 2] has generated renewed interest in this century-old topic. It is now well understood that the system presented in [1] entailed several key design elements. First, a helix structure of resonant length excited through a primary coupling loop was used on both the transmitter and the receiver. Careful tuning of the coupling loop was essential for impedance matching, since in order to achieve a high power transfer efficiency, the load impedance must be well matched to the so-called Linville load of the two-port network [3, 4] (which can equivalently be derived from the simultaneous conjugate matching condition [5, 6]). Finally, thick wires were used to achieve low conductor loss, a key consideration to maintaining high power transfer efficiency. Subsequently, a capacitor-loaded loop structure was proposed in [2] to further confine the electric field at resonance to the capacitor. The motivation for this was so that the fields in the air become primarily magnetic and would interact less with nearby dielectric materials.

Since then, there has been strong interest in the application of WPT to charging electrical and electronic devices. This has generated much recent work to design WPT structures in a reduced form factor [7–17]. For example, the use of spiral resonators has been investigated in [7–12]. Alternatively, a capacitor-loaded loop structure may be used as the resonator [13–17]. In this paper, we expand upon the design in [16] and investigate a planarized, capacitor-loaded coupled loop structure for WPT. First, we show that the optimal configuration for the traditional capacitor-loaded coupled loop structure (Fig. 1) occurs when the coupled loops are coplanar. Next, by converting thick wires into wide strips, we achieve a planarized configuration. Simulation results are verified in measurement and the contribution of different loss mechanisms are examined. To further characterize the properties of the design, we investigate the transmission efficiency in the presence of dielectric materials via simulation and measurement. Tuning capabilities that arise from the implementation of a variable capacitor are presented. Finally, design space exploration is performed to investigate design tradeoffs between size, frequency, and transmission distance.

Received 17 July 2014, Accepted 10 August 2014, Scheduled 20 August 2014

* Corresponding author: Chenchen Jimmy Li (cjli@utexas.edu).

The authors are with the Department of Electrical and Computer Engineering, The University of Texas at Austin, Austin, TX 78701, USA.

2. DESIGN EVOLUTION

We begin with the design evolution starting from the standard capacitor-loaded coupled loop configuration shown in Fig. 1 toward a planar design. The initial structure consists of identical structures for both the transmitter (Tx) and the receiver (Rx). Each consists of a smaller primary loop and a larger, capacitor-loaded secondary loop. The secondary loop has a radius of 0.30 m and is loaded by a capacitor to generate resonance at 6.78 MHz. Thick copper wire of radius 8.08 mm is used for the secondary loop while the primary loop uses thin wire of radius 0.512 mm, as the majority of the current flows on the secondary loop [18]. Both the source and load impedances are assumed to be 50 Ω. Here, we define power transfer efficiency (PTE) as the ratio of the power dissipated in the 50 Ω load to the available power at the Tx input (or the $|S_{21}|^2$ of the two-port network). Our design focuses on optimizing PTE at a distance of 1 m.

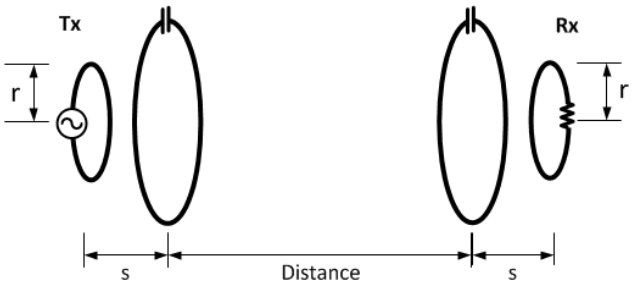

Figure 1. Basic structure for wireless power transfer via capacitor-loaded coupled loops.

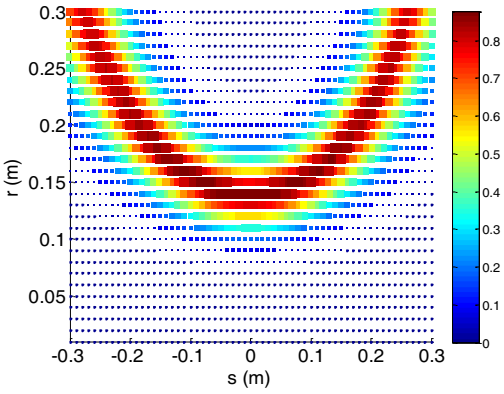

Figure 2. PTE at 1 m distance vs. the primary loop radius (r) and the spacing between primary and secondary loops (s).

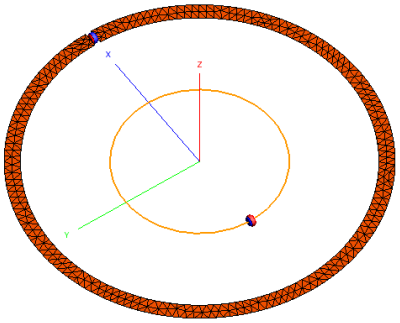

(a)

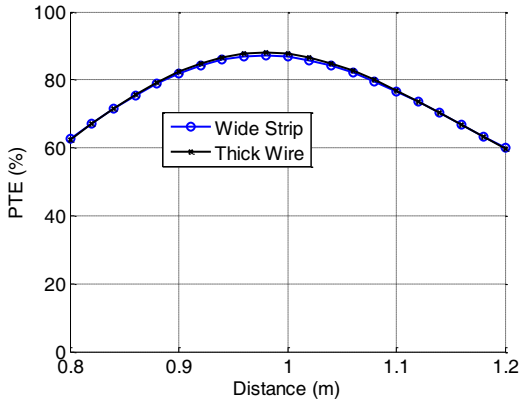

(b)

Figure 3. (a) Planarized wide strip model. (b) PTE of thick wire and wide strip model.

Simulation and optimization of the primary loop radius (r) and the spacing between the primary and secondary loop (s) are carried out using FEKO [19]. Fig. 2 shows a color plot of the PTE at 1 m for different combinations of r and s. It is interesting to see that the maximum PTE in this plot occurs when the primary loop radius $r = 0.14$ m and the primary loop is coplanar with the secondary loop ($s = 0$ m). This indicates the optimal structure can be readily planarized.

Next, we convert thick wire into wide strips to achieve a planar Tx and Rx structure. The following equation is used to convert the thick wire into an equivalent conducting strip:

$$2 * width = 2\pi r_{wire} \tag{1}$$

A factor of two is present on the left side to account for the current flow on both sides of the conducting strip. Based on Eq. (1), the thick wire of the secondary loop is converted into a 1″-wide coplanar strip whose FEKO simulation model is shown in Fig. 3(a). FEKO simulated PTE values of a thick wire implementation and a wide strip implementation are compared in Fig. 3(b). The two results are nearly identical, supporting the use of Eq. (1) in converting the wire design to a strip form. Note that current crowding at the edges of the strip may limit the power handling capability of the strip when compared to the thick wire. This additional factor should be taken into consideration in the design.

3. MEASUREMENT VERIFICATION

Next, we construct a prototype and compare the PTE measurement results with that of FEKO simulation. The prototype is constructed using thin 18 AWG wire for the primary loop and a 0.02″-thick and 1″-wide copper sheet ring cutout for the secondary loop. The ring structure is split and a variable capacitor (Sprague-Goodman, Q-factor = 650) is soldered in series. The variable capacitors are manually tuned to resonate each loop at 6.78 MHz. Fig. 4 shows the measurement setup for S_{21} measurements using a vector network analyzer. PTE measurements between the Tx and Rx structures are done at discrete distances from 0.80 m to 1.20 m. Two 2 : 1 transformer baluns [4] were used initially. However, measurement results showed no difference with or without the baluns. This may be due to the low operating frequency and the electrically small, non-radiative nature of the loop. No balun was used in subsequent measurements.

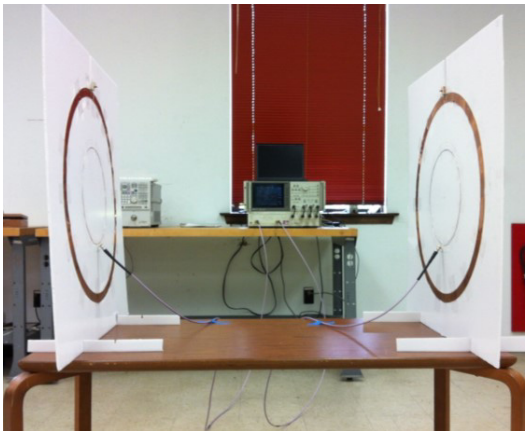

Figure 4. Measurement setup of prototype.

FEKO simulation is done using identical copper Tx and Rx structures (shown in Fig. 3(a)). Each capacitor is set to resonate the loop at 6.78 MHz. A series resistance is added to simulate the finite quality factor of the capacitor — defined as the ratio of the absolute value of the reactance to that of the equivalent series resistance and is approximated by [5, 20]:

$$R_c = \frac{1}{\omega_0 Q C} \tag{2}$$

where Q is assumed to be 650 based on manufacturer's spec sheet, ω_0 the resonant frequency of the system, and C the capacitance value needed to resonate the loop.

Figure 5 shows the measurement and simulation results. The measurement results are shown as black dots. Plotted for comparison are two FEKO simulation results. The dashed red curve uses a lossless capacitor and the solid blue curve includes an additional series resistance for a capacitor with Q-factor of 650 based on Eq. (2). Fig. 5(a) shows PTE vs. frequency with Tx and Rx at 1 m distance. There is good agreement between measurement and the finite-Q capacitor simulation. More than 60% efficiency is achieved in measurement at 6.75 MHz. It also illustrates the high-Q nature of the design. Fig. 5(b) shows PTE vs. distance at the peak PTE frequency. Again, there is good agreement between measurement and simulation — the measurement result being slightly higher suggests that the capacitor

Q-factor is slightly higher than 650. This result also shows the geometry is only optimized for a specific distance, although the drop-off around the 1 m target distance is moderate.

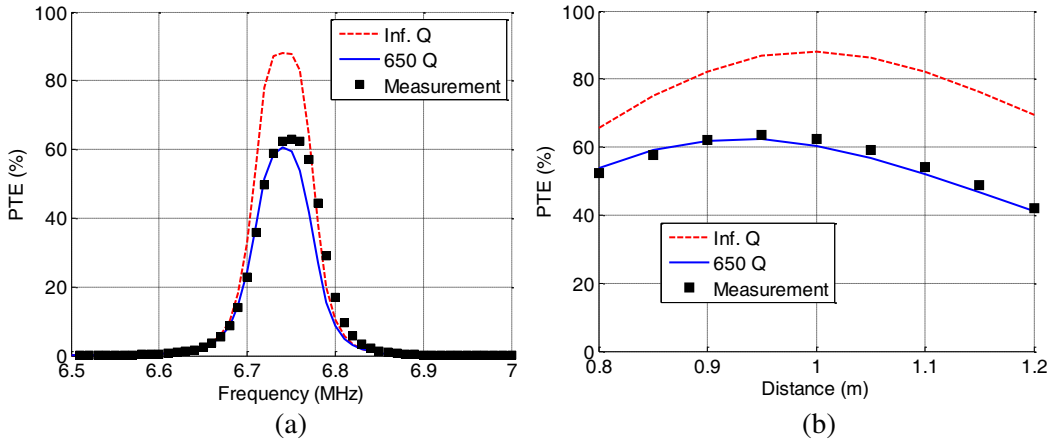

Figure 5. (a) PTE vs. frequency at 1 m. (b) PTE vs distance at resonance.

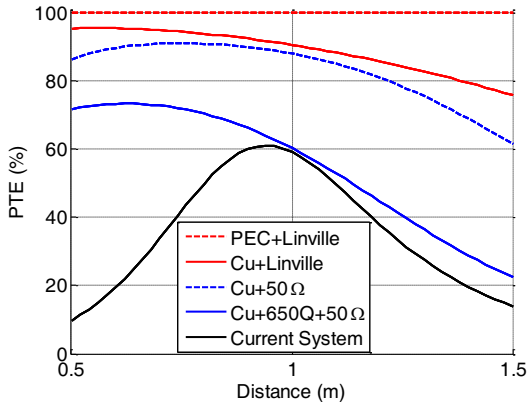

Figure 6. PTE with inclusion of different loss mechanisms.

Next, we examine the contribution of various loss mechanisms on the PTE of the system. A theoretical bound for WPT in the near-field region was derived in [6]. At a distance of 1 m, or less than a tenth of a wavelength at 6.78 MHz, the theoretical bound from [6] is essentially 100%. To approach this, we must remove all sources of loss in the system. These are input and load mismatch losses, wire resistive loss, and capacitor resistive loss. Radiation resistance is considered negligible due to the electrically small loop. Fig. 6 shows the contribution of each source of loss through FEKO simulation. The black curve is the current system with all sources of loss considered. At a transmission distance of 1 m, 59% transmission efficiency is achieved. The blue curve discounts input mismatch and achieves 60% efficiency. The dashed blue curve additionally discounts capacitor loss and achieves 88% efficiency. The red curve also discounts load mismatch (using the Linville load for each transmission distance) and achieves 91% efficiency. Finally, the dashed red curve additionally discounts conductor loss and thus reaches 100% efficiency. Based on these numbers, we see that the 41% total loss in efficiency can be broken down into: 1% input mismatch, 28% capacitor loss, 3% load mismatch, and 9% conductor loss of the loops. Therefore, the most dominant loss factor in the transfer efficiency of the overall system is the finite Q-factor of the capacitor. An improved quality factor on the capacitor could further enhance the transfer efficiency into the $> 80\%$ range.

4. MATERIAL EFFECTS

While the capacitor is a key source of loss, it confines the electric field at resonance. Therefore, nearby dielectric materials are not expected to strongly affect the resonant frequency or lower the PTE [2]. To verify this, we first examine the stored electric and magnetic energy in free space at resonance in FEKO simulation. To save simulation time, the equivalent thick wire model was used for the structure. The stored electric and magnetic field are examined in two different regions of the WPT system. Fig. 7 shows the simulation setup where the highlighted $0.6\,\text{m} \times 0.6\,\text{m} \times 0.6\,\text{m}$ or $(0.6\,\text{m})^3$ region of space is examined. A 1 V drive is applied at the input. To evaluate the stored magnetic and electric energy in free space, the following two expressions are used:

$$W_E = \iiint \frac{1}{2}\varepsilon_0 |E|^2 dv \tag{3}$$

$$W_H = \iiint \frac{1}{2}\mu_0 |H|^2 dv \tag{4}$$

The points are uniformly sampled in a $(0.6\,\text{m})^3$ volume and integrated using a midpoint Riemann sum. In the region in Fig. 7(a), the stored magnetic energy is three orders of magnitude greater than that of the stored electric energy (1183 pJ and 3 pJ respectively). In the region in Fig. 7(b), the stored magnetic energy is one order of magnitude greater than that of the stored electric energy (25 pJ and 1 pJ respectively). At resonance the total stored electric energy and magnetic energy in the system are equal. Therefore, these numbers confirm that most of the stored electric energy is confined to the capacitor and not distributed in air. Moreover, the stored magnetic energy is concentrated in the region between the Tx and Rx.

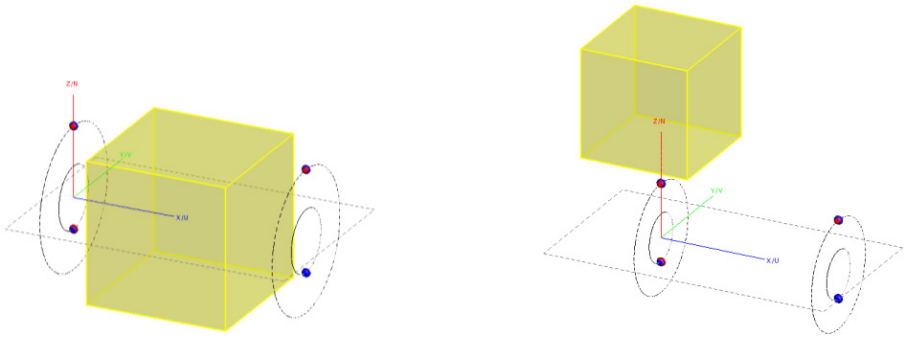

(a) (b)

Figure 7. FEKO stored near-field energy simulation setup. (a) Region between transmitter and receiver. (b) Region to the side of transmitter.

Next, the effect of dielectric materials on PTE is examined. We vary both the dielectric constant and the conductivity of the material. Fig. 8(a) shows the simulation done in FEKO using a $0.60\,\text{m} \times 0.60\,\text{m} \times 0.25\,\text{m}$ dielectric cuboid placed in between the transmitter and receiver (spaced 1 m apart). Fig. 8(b) shows the resulting PTE values for materials of different dielectric constants and conductivity. For a given dielectric constant, the PTE is found for conductivity from 0 to 1.5 S/m. The plot shows no change in PTE from a change in dielectric constant but degrades due to increasing conductivity. This is due to the time-varying magnetic field generating eddy currents in the material through its conductivity. Therefore, lossy dielectric materials would, in general, cause a degradation in the PTE for magnetically coupled WPT system.

To verify this effect in measurement, water with varying salinity is used as a dielectric with varying conductivity. A foam container is filled with water and centered in between the Tx and Rx that are spaced 1 m apart. Fig. 9 shows the measurement setup with foam blocks to support the container. The volume of water in the container is $0.34\,\text{m} \times 0.26\,\text{m} \times 0.14\,\text{m}$.

At 6.78 MHz, tap water has almost no conductivity. By incrementally dissolving salt into the water, the salinity of the water can be increased from 0 parts per thousand (ppt) to 40 ppt. This

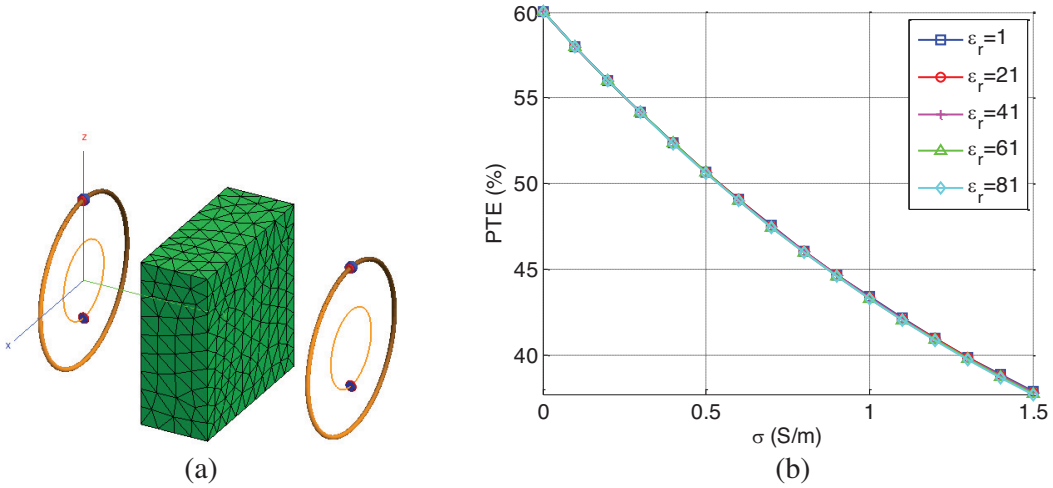

Figure 8. (a) FEKO materials simulation setup. (b) PTE vs. relative permittivity and conductivity.

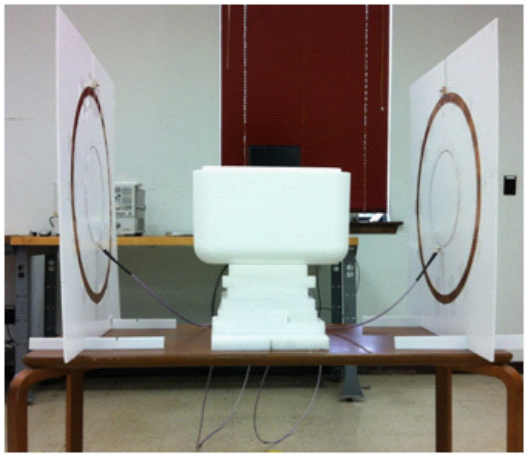

Figure 9. PTE measurement setup with water.

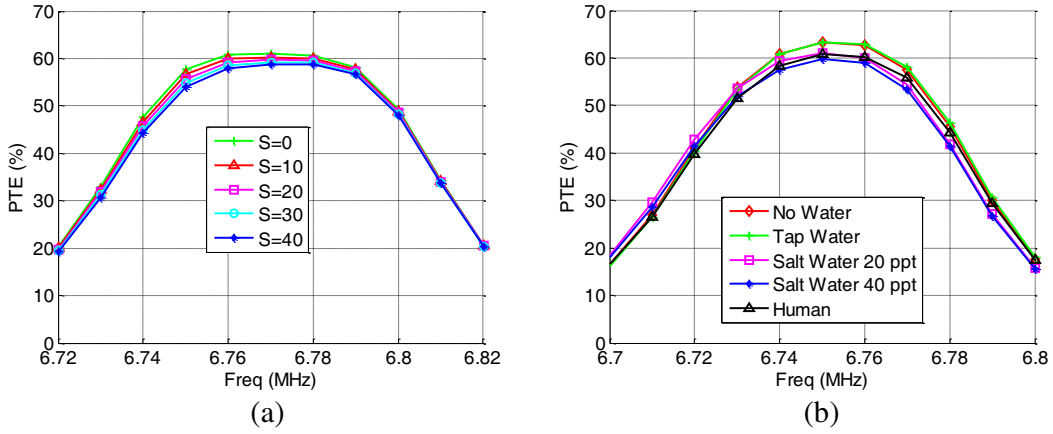

Figure 10. (a) PTE simulation with water. (b) PTE measurement with water.

results in an increase of conductivity from 0 to 4.3 S/m based on [21]. Fig. 10(a) shows the simulated PTE using water with varying salinity from 0 to 40 ppt. Fig. 10(b) shows the measured PTE using

no water, tap water, water with salinity of 20 ppt, and water with salinity of 40 ppt. The simulated results in Fig. 10(a) show a small decrease in PTE as the salinity increases. This trend is corroborated in measurement in Fig. 10(b). Additionally, a measurement was done with a person (the first author) in between transmitter and receiver with efficiency loss that falls between that of 20 and 40 ppt. Notice that there is a significant difference in efficiency loss between Fig. 8 and Fig. 10. This is due to the large difference in volume (7.3 times). Additionally, while the average human torso is approximately 0.60 m × 0.60 m × 0.25 m, the volume is not a homogenous lossy liquid. Therefore, the degradation due to a human is much smaller than what Fig. 8 implies. Overall, the structure proved robust to the presence of medium-sized dielectric objects.

5. TUNING CAPABILITIES

We next examine the tuning capabilities offered by the variable capacitors in the system. For simplicity, we fix the loss resistance of the capacitors. First, simultaneous tuning of the Tx and Rx capacitors allows for resonant frequency tuning. In FEKO simulation, the structure geometry and distance are fixed and only the capacitance of each loop is varied from 230 pF to 593 pF. The frequency adjustable nature of the system is illustrated in the distinct frequency peaks in Fig. 11(a). The resulting peak PTE varies between 55% at 5.5 MHz to 65% at 9 MHz. This result shows that although the system was designed specifically for 6.78 MHz, the frequency of operation can be tuned from 5.5 MHz to 9 MHz without large variations in the PTE.

A second, more interesting idea is to use the variable capacitors to alleviate the mismatch loss due to distance variation. Earlier, Fig. 5(b) showed the drop-off in PTE away from the 1 m design distance. Here, simulation is carried out for different distances and capacitances. Fig. 11(b) shows a color plot of PTE at 6.78 MHz versus distance and capacitance. If we fix the capacitance value at 395 pF, a drop-off in PTE away from 1 m similar to that shown in Fig. 5(b) is observed. However, if we follow the tilted ridge in dark red (61% at 1 m and 395 pF, 63% at 0.75 m and 388 pF, and 65% at 0.5 m and 381 pF), higher PTE can be maintained. Therefore, by simultaneously tuning the variable capacitor of both the Tx and Rx, improved matching and higher PTE can be obtained at distances closer than 1 m. This approach is different from the frequency-tracking technique in [7, 9] where the source frequency is changed to track the resonant frequency-splitting that occurs when Tx and Rx are close. Instead, the source frequency can be kept constant while both capacitors are tuned to track the distance-varying input impedance.

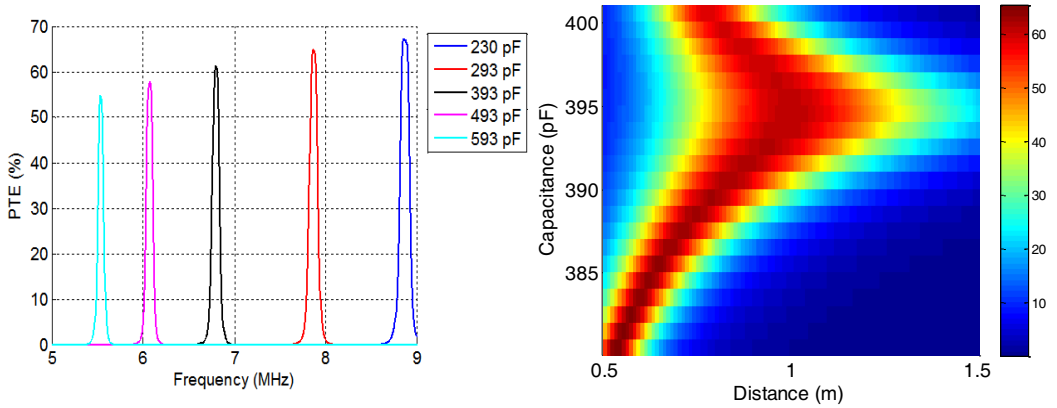

Figure 11. (a) Resonant frequency tuning. (b) Impedance match tuning for variable distance.

6. DESIGN SPACE EXPLORATION

Finally, the previous design constraints in frequency, target distance, and size of the structure are removed so that their effects on PTE can be more fully investigated. Again, the loss resistance of the

capacitor is fixed for simplicity. For each case, one parameter is fixed while the other two are altered. At each point in the sweep, the primary loop radius is re-optimized to achieve impedance matching (the design is kept planar). By doing so, we can better identify the design trade-offs between size, resonant frequency, transmission distance, and PTE.

First, target distance and structure size (dictated by the secondary loop radius) are allowed to vary while frequency is fixed at 6.78 MHz. Intuitively, it is expected that decreasing the size of the structure would also decrease the distance at which efficient transfer can be maintained. Fig. 12(a) is a contour plot of the PTE versus the target distance and secondary loop radius. It is shown there is a direct relationship between the target distance and the secondary loop radius to maintain the same efficiency. As expected, higher efficiency can be attained at a shorter transmission distance for a fixed loop radius.

Second, the target distance is fixed at 1 m while size and frequency are swept. In Fig. 12(b), there is an inverse relationship between size and frequency such that in order to decrease size, an increase in frequency is required to maintain the same efficiency. This is slightly counter-intuitive since increasing the frequency also increases the electrical distance the loops are spaced apart. However, increasing the frequency increases the electrical size of the loops (though not large enough that radiation resistance becomes relevant). This also means that, for a fixed size, increasing the frequency tends to increase the efficiency. This explains the increasing PTE with frequency observed in Fig. 11(a).

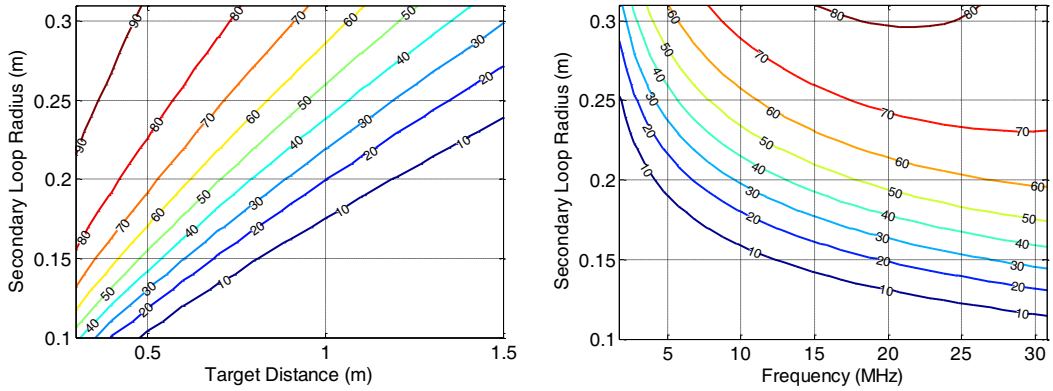

Figure 12. (a) PTE vs. size and target distance. (b) PTE vs. size and frequency.

7. CONCLUSION

In this paper, we have demonstrated that the optimal configuration for the traditional capacitor-loaded coupled loop structure is when the coupled loops are coplanar and that by implementing wide strips in place of thick wires, the structure can be planarized. The chosen design constraints were a resonant frequency of 6.78 MHz, a maximum loop diameter of 0.6 m, and a target transfer distance of 1 m. Measurement results showed efficiency of 60% at 1 m distance that was limited by the Q-factor of the capacitor.

Investigation of the material effects of this structure revealed that it is robust to the presence of medium-sized dielectric objects. Additionally, it was shown that a variable capacitor can be used for tuning purposes in two forms. First, the resonant frequency can be tuned without changing the physical geometry. Second, the target distance can be adjusted without changing the resonant frequency. Finally, design space exploration revealed that, in order to maintain the same efficiency, there is a direct relationship between Tx/Rx size and the transmission distance and an inverse relationship between the Tx/Rx size and operating frequency.

REFERENCES

1. Kurs, A., A. Karalis, R. Moffatt, J. D. Joannopoulos, P. Fisher, and M. Soljačić, "Wireless power transfer via strongly coupled magnetic resonances," *Science*, Vol. 317, No. 5834, 83–86, Jul. 2007.

2. Karalis, A., J. D. Joannopoulos, and M. Soljačić, "Efficient wireless non-radiative mid-range energy transfer," *Ann. of Phys.*, Vol. 323, No. 1, 34–48, Jan. 2008.
3. Balanis, C. A., *Antenna Theory: Analysis and Design*, 2nd Edition, Sec. 8.5, Wiley, New York, 1997.
4. Yoon, I.-J. and H. Ling, "Realizing efficient wireless power transfer using small folded cylindrical helix dipoles," *IEEE Antennas Wireless Propag. Lett.*, Vol. 9, 846–849, Sep. 2010.
5. Pozar, D. M., *Microwave Engineering*, 3rd Edition, Wiley, New Jersey, 2004.
6. Lee, J. and S. Nam, "Fundamental aspects of near-field coupling small antennas for wireless power transfer," *IEEE Trans. Antennas Propagat.*, Vol. 58, No. 11, 3442–3449, Nov. 2010.
7. Sample, A. P., D. A. Meyer, and J. R. Smith, "Analysis, experimental results, and range adaptation of magnetically coupled resonators for wireless power transfer," *IEEE Trans. Ind. Electron.*, Vol. 58, No. 2, 544-554, Feb. 2011.
8. Klein, A. and N. Katz, "Strong coupling optimization with planar resonators," *Curr. Appl. Phys.*, Vol. 11, No. 5, 1188–1191, Feb. 2011.
9. Park, J., Y. Tak, Y. Kim, Y. Kim, and S. Nam, "Investigation of adaptive matching methods for near-field wireless power transfer," *IEEE Trans. Antennas Propag.*, Vol. 59, No. 5, 1769–1773, May 2011.
10. Kim, H. and H. Lee, "Design of an integrated wireless power transfer system with high power transfer efficiency and compact structure," *Proc. EuCAP*, 3627–3630, Prague, Czech Republic, Mar. 2012.
11. Xue, R.-F., K.-W. Cheng, and M. Je, "High-efficiency wireless power transfer for biomedical implants by optimal resonant load transformation," *IEEE Trans. Circuits Syst. I*, Vol. 60, No. 4, 867–874, Apr. 2013.
12. Jonah, O., A. Merwaday, S. V. Georgakopoulos, and M. M. Tentzeris, "Spiral resonators for optimally efficient strongly coupled magnetic resonance systems," *Wireless Power Transfer J.*, Vol. 1, No. 1, 21–26, Mar. 2014.
13. Choi, J. and C. H. Seo, "Analysis on transmission efficiency of wireless energy transmission resonator based on magnetic resonance," *Progress In Electromagnetics Research M*, Vol. 19, 221–237, 2011.
14. Komaru, T., M. Koizumi, K. Komurasaki, T. Shibata, and K. Kano, "Compact and tunable transmitter and receiver for magnetic resonance power transmission to mobile objects," *Wireless Power Transfer — Principles and Engineering Exploration*, K. Y. Kim, Ed., 130–150, InTech, 2012.
15. Jolani, F., J. Mehta, Y. Yu, and Z. Chen, "Design of wireless power transfer systems using magnetic resonance coupling for implantable medical devices," *Progress In Electromagnetics Research Letters*, Vol. 40, 141–151, 2013.
16. Li, C. J. and H. Ling, "A planarized, capacitor-loaded loop structure for wireless power transfer," *IEEE Antennas Propag. Int. Symp.*, 840–841, Orlando, FL, Jul. 2013.
17. Tierney, B. and A. Grbic, "Planar shielded-loop resonators," *IEEE Trans. Antennas Propagat.*, Vol. 62, No. 6, 3310–3320, Jun. 2014.
18. Sugiyama, H., "Performance analysis of magnetic resonance system based on electrical circuit theory," *Wireless Power Transfer — Principles and Engineering Exploration*, K. Y. Kim, Ed., 95–116, InTech, 2012.
19. FEKO Version 6.0, EM Software & Systems-S.A., Stellenbosch, South Africa, 2010 [Online]. Available: http://www.feko.info.
20. Di Paulo, F., *Networks and Devices Using Planar Transmission Lines*, 490–491, CRC Press LLC, Boca Raton, 2000.
21. Meissner, T. and F. J. Wentz, "The complex dielectric constant of pure and sea water from microwave satellite observations," *IEEE Trans. Geosci. Remote Sens.*, Vol. 42, No. 9, 1836–1849, Sep. 2004.